Reducing unitary coupled cluster circuit depth by classical stochastic amplitude prescreening

Maria-Andreea Filip [1,*] Nathan Fitzpatrick,[2,†] David Muñoz Ramo,[2] and Alex J. W. Thom [1,‡]
[1]*Yusuf Hamied Department of Chemistry, Lensfield Road, CB2 1EW Cambridge, United Kingdom*
[2]*Cambridge Quantum Computing Ltd., 13-15 Hills Road, CB2 1NL Cambridge, United Kingdom*

(Received 10 September 2021; accepted 24 May 2022; published 27 June 2022)

Unitary coupled cluster (UCC) approaches are an appealing route to utilizing quantum hardware to perform quantum chemistry calculations, as quantum computers can in principle perform UCC calculations in a polynomially scaling fashion, as compared with the exponential scaling required on classical computers. Current noisy intermediate scale quantum computers are limited by both hardware capacity in number of logical qubits and the noise introduced by the deep circuits required for UCC calculations using the variational quantum eigensolver (VQE) approach. We present a combined classical-quantum approach where a stochastic classical UCC preprocessing step is used to determine the important excitations in the UCC *Ansatz*. The reduced number of selected excitations are then used in a UCC-based VQE calculation. This approach gives a systematically improvable approximation, and we show that significant reductions in quantum resources can be achieved, with simulations on the CH_2, N_2, and N_2H_2 molecules giving submillihartree errors.

DOI: 10.1103/PhysRevResearch.4.023243

I. INTRODUCTION

Quantum chemistry, which often concerns itself with solutions to problems with exponentially scaling Hilbert spaces, has long been identified as a good target for quantum computation, which would allow the encoding of such problems in a linear number of qubits. For example, algorithms such as quantum phase estimation [1,2] have been suggested as means of efficiently computing the ground state energies of molecular systems [3]. However, this approach would require fault-tolerant quantum computers. In the current noisy intermediate-scale quantum (NISQ) regime, the field of quantum chemistry calculations on quantum computers is dominated by hybrid quantum-classical approaches and particularly the variational quantum eigensolver (VQE) [4], which requires a parameterized wave function. Various parameterized *Ansatz* schemes have been proposed, such as the hardware-efficient *Ansatz* [5], the hardware-variational *Ansatz* [6], the symmetry-preserving *Ansatz* [7], and the unitary coupled cluster (UCC) *Ansatz* [8–11]. UCC has seen a resurgence as a convenient parametrization for VQE [4,12] due to its ability to be easily encoded into a quantum circuit. While its physical origin leads to a series of appealing features, including a relatively well-behaved energy landscape, the qubit encoding of the fermionic operators in the UCC *Ansatz* produces very deep circuits, which are challenging for currently available quantum architectures. Work has been done to decrease the depth of these circuits while maintaining the physicality of the *Ansatz*, for example, by using Moller-Plesset [13] (MP2) theory results to screen amplitudes [14,15] or using adaptive *Ansätze* such as ADAPT-VQE [16]. While the latter does generate shorter, highly accurate *Ansätze*, it does so at the cost of an increased number of measurements relative to the standard UCC approach. Other approaches which select contributing amplitudes based on their energy gradient have been developed, such as qubit coupled cluster [17,18] or energy-sorted UCC [19], but like ADAPT-VQE, they require additional quantum computation to obtain the screened set of operators.

In this paper, we propose using the recently developed UCC Monte Carlo [20] (UCCMC) approach to screen amplitudes for a UCC-based VQE calculation. Quantum Monte Carlo (QMC) methods [21,22] take advantage of the sparsity of most chemical Hamiltonians to generate compact wave functions, thereby lowering memory requirements relative to the corresponding classical algorithms. Additionally, the Monte Carlo (MC) approach naturally samples important contributions to the wave function—determinants with large Hamiltonian coupling terms to the reference determinant—first, and therefore, while fully converging a QMC calculation may be time consuming, short runs may be used to quickly identify the most important contributions to a given wave function [23]. We use this property of the UCCMC method and particularly its Trotterized approximation to provide an initial set of amplitudes for a VQE calculation. We screen amplitudes based on these initial values and assess the effect of using the screened parameter sets on the accuracy of the obtained energy, comparing with the equivalent result from MP2 screening.

*maf63@cam.ac.uk
†nathan.fitzpatrick@cambridgequantum.com
‡ajwt3@cam.ac.uk

In Sec. II, we review the underlying theory of both the UCC-based VQE and the UCCMC method. Section III comprises results and discussion for a range of small molecules in a variety of scenarios, and Sec. IV presents our conclusions.

II. THEORY

Coupled cluster (CC) theory [24,25] has become well established as the gold standard of *ab initio* quantum chemistry methods. The exponential *Ansatz*:

$$|\Psi_{\mathrm{CC}}\rangle = \exp(\hat{T})\,|\Psi_0\rangle\,, \tag{1}$$

where $\hat{T} = \sum_i \hat{T}_i$, and $\hat{T}_i$ is composed of all valid excitation operators of order i, naturally maintains size-consistency when the operator $\hat{T}$ is truncated at some excitation level, with the most commonly employed truncations being CC singles and doubles (CCSD) and CC singles, doubles, and triples (CCSDT). Such methods are polynomially scaling with system size and systematically improvable, both highly desirable properties. However, the exponential operator in this form is nonunitary, and therefore, it cannot be directly implemented on a quantum computer.

A. The UCC *Ansatz*

We can construct the anti-Hermitian operator $\hat{T} - \hat{T}^\dagger$, the exponential of which gives a unitary operator. The UCC wave function is therefore

$$|\Psi_{\mathrm{UCC}}\rangle = \exp(\hat{T} - \hat{T}^\dagger)|\Psi_0\rangle, \tag{2}$$

and its energy can be found variationally as

$$E_0 = \min_{\mathbf{t}} \langle\Psi_0|\exp[-(\hat{T} - \hat{T}^\dagger)]\hat{H}\exp[\hat{T} - \hat{T}^\dagger]|\Psi_0\rangle. \tag{3}$$

Although $\exp[-(\hat{T} - \hat{T}^\dagger)]\hat{H}\exp(\hat{T} - \hat{T}^\dagger)$ has a nonterminating Baker-Campbell-Hausdorff expansion, which makes the implementation of UCC costly on a classical computer, the unitary operator $\exp(\hat{T} - \hat{T}^\dagger)$ can be decomposed as a series of universal quantum gates on a quantum computer. We start by writing the cluster operator in terms of individual excitations:

$$U(\mathbf{t}) = \exp\left[\sum_{\mathbf{n}} t_{\mathbf{n}}(\hat{\tau}_{\mathbf{n}} - \hat{\tau}_{\mathbf{n}}^\dagger)\right], \tag{4}$$

where $\tau_{\mathbf{n}}$ represents a fermionic excitation operator and $t_{\mathbf{n}}$ its corresponding cluster amplitude. We can take a Trotter-Suzuki expansion [26,27] of $U(\mathbf{t})$ such that

$$|\Psi_{\mathrm{UCC}}\rangle \approx |\Psi_{\mathrm{tUCC}}\rangle = \left(\prod_{\mathbf{n}} \exp\left[\frac{t_{\mathbf{n}}}{\rho}(\hat{\tau}_{\mathbf{n}} - \hat{\tau}_{\mathbf{n}}^\dagger)\right]\right)^{\rho} |\Psi_0\rangle, \tag{5}$$

with equality achieved as $\rho \to \infty$. We can take $\rho = 1$, which has been shown [12] to be a good approximation, leading to negligible errors in the resulting energy, to obtain

$$|\Psi_{\mathrm{tUCC}}\rangle \approx U_1(\mathbf{t})|\Psi_0\rangle = \prod_{\mathbf{n}} \exp[t_{\mathbf{n}}(\hat{\tau}_{\mathbf{n}} - \hat{\tau}_{\mathbf{n}}^\dagger)]|\Psi_0\rangle, \tag{6}$$

also known as the disentangled UCC *Ansatz* [28]. For the case of UCCSD, the singles are represented by

$$\hat{T}_1 = \sum_{i,\alpha} t_i^\alpha(\hat{a}_i^\dagger\hat{a}_\alpha - \hat{a}_\alpha^\dagger\hat{a}_i), \tag{7}$$

and doubles are represented by

$$\hat{T}_2 = \sum_{i>j,\alpha>\beta} t_{ij}^{\alpha\beta}(\hat{a}_\alpha^\dagger\hat{a}_\beta^\dagger\hat{a}_i\hat{a}_j - \hat{a}_j^\dagger\hat{a}_i^\dagger\hat{a}_\alpha\hat{a}_\beta), \tag{8}$$

where the Latin indices represent occupied spin orbitals, and the Greek indices represent virtual spin orbitals. This can be easily implemented on a quantum computer via an appropriate transformation of the fermionic operators to the unitary bosonic qubit operators using schemes like Jordan-Wigner [29] or Bravyi-Kitaev [30], where algebraic compilation strategies based on the ZX calculus have been proposed [31].

B. Quantum computing and the UCC *Ansatz*

NISQ hardware is characterized by small qubit counts and high noise levels due mainly to short qubit coherence times, quantum gate errors, faulty readout operations, and crosstalk between qubits during operation. These limitations prevent the use of error-correction protocols that would enable large quantum computations. Thus, it is advantageous to reduce the amount of quantum computation to a minimum. As a result, there is a strong research effort dedicated to the development of hybrid quantum-classical algorithms. One of the main algorithmic workhorses of this field is the VQE [4], where a minimizer run on a classical machine optimizes a cost function evaluated by the quantum computer. In chemistry problems, this corresponds to finding the expected value of the energy with respect to a parameterized *Ansatz* wave function. Alternative approaches have appeared in recent years; we highlight methods based on imaginary time propagation of a trial wave function, either via a variational principle [32] or approximating the nonunitary evolution with an appropriate quantum circuit [33], and techniques to variationally optimize the reduced density matrix of the system [34].

The UCC *Ansatz* is attractive for this kind of quantum algorithm, as it has a reduced number of parameters to optimize and a more favorable energy-search landscape compared with hardware-tailored *Ansätze* [5]. It also naturally conserves the number of electrons and the M_z spin projection quantum number during the calculation, thus helping to prevent convergence to unwanted states or avoiding the barren plateau problem observed for hardware-efficient *Ansätze* [35]. However, these advantages are obtained at the cost of large circuit depths. For example, in the Jordan-Wigner mapping, fermionic creation and annihilation operators may be expressed as

$$\hat{a}_j^\dagger = \bigotimes_i^{j-1} Z_i \bigotimes \frac{1}{2}(X_j - iY_j), \tag{9}$$

$$\hat{a}_j = \bigotimes_i^{j-1} Z_i \bigotimes \frac{1}{2}(X_j + iY_j). \tag{10}$$

Therefore, a single fermionic excitation operator becomes

$$t_i^\alpha(\hat{a}_i^\dagger\hat{a}_{\hat{a}} - \hat{a}_{\hat{a}}^\dagger\hat{a}_i) = \frac{it_i^\alpha}{2}\bigotimes_{k=i+1}^{\alpha-1} Z_k(Y_iX_\alpha - X_iY_\alpha), \tag{11}$$

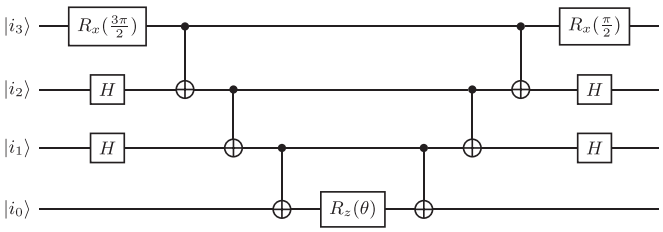

FIG. 1. Pauli gadget for $\exp[-i\frac{\theta}{2}(Z_0 \otimes X_1 \otimes X_2 \otimes Y_3)]$.

while a double excitation is given by

$$t_{ij}^{\alpha\beta}(\hat{a}_\alpha^\dagger \hat{a}_\beta^\dagger \hat{a}_i \hat{a}_j - \hat{a}_j^\dagger \hat{a}_i^\dagger \hat{a}_\alpha \hat{a}_\beta) = \frac{it_{ij}^{\alpha\beta}}{8} \bigotimes_{k=i+1}^{j-1} Z_k \bigotimes_{l=\alpha+1}^{\beta-1} Z_l (X_i X_j Y_\alpha X_\beta + Y_i X_j Y_\alpha Y_\beta + X_i Y_j Y_\alpha Y_\beta + X_i X_j X_\alpha Y_\beta - Y_i X_j X_\alpha X_\beta - X_i Y_j X_\alpha X_\beta - Y_i Y_j Y_\alpha X_\beta - Y_i Y_j X_\alpha Y_\beta). \quad (12)$$

Therefore, each excitation included in the *Ansatz* contributes with a series of Pauli gadgets (see Fig. 1), requiring a large number of two-qubit gates. These gates are responsible for most of the noise produced during a quantum computation on NISQ devices, so it is very important to reduce their number. The ability to identify which excitations have a negligible contribution to the total energy would enable their elimination in the *Ansatz* and reduce the overall circuit depth of the state preparation step in variational quantum algorithms. Successful screening of excitations aims to bring the circuit execution time within the coherence time of near-term hardware with maximal fidelity with the unscreened *Ansatz*, incurring a minimum energy penalty.

C. QMC algorithms

MC algorithms have become popular approaches to more effectively use classical computational resources for quantum chemistry. Real-space approaches such as diffusion MC (DMC) [36,37] suffer from the so-called *sign problem*, which causes them to naturally converge to bosonic solutions. This can be somewhat mitigated by using arbitrary nodal surfaces; however, this introduces an uncontrolled approximation. Recently, Hilbert space QMC methods have been developed that naturally avoid the DMC sign problem. Full configuration QMC (FCIQMC) [21] encodes a stochastic solution to the full configuration interaction (FCI) equation. The FCI wave function is expressed as a linear combination of a reference determinant [usually the Hartree-Fock (HF) wave function] and all possible excited determinants starting from it:

$$|\Psi_{\mathrm{FCI}}\rangle = (1 + \hat{C})\,|D_0\rangle\,, \quad (13)$$

where $\hat{C} = \sum_{i,\alpha} C_i^\alpha \hat{a}_i^\alpha + \frac{1}{4}\sum_{i,j,\alpha,\beta} C_{ij}^{\alpha\beta}\hat{a}_{ij}^{\alpha\beta} + ...$, and $\hat{a}_i^\alpha, \hat{a}_{ij}^{\alpha\beta}$ are excitation operators. The coefficients $\mathbf{C}$ can be optimized by minimizing the energy with respect to them. This gives the following set of equations:

$$\langle D_{\mathbf{i}}|\hat{H} - E|\Psi_{\mathrm{FCI}}\rangle = 0, \quad (14)$$

where $|D_{\mathbf{i}}\rangle$ span the full Hilbert space of the system. Equivalently,

$$\langle D_{\mathbf{i}}|1 - \delta\tau(\hat{H} - E)|\Psi_{\mathrm{FCI}}\rangle = \langle D_{\mathbf{i}}|\Psi_{\mathrm{FCI}}\rangle\,, \quad (15)$$

which can be written in an iterative form as

$$C_{\mathbf{i}}(\tau) - \delta\tau\,\langle D_{\mathbf{i}}|\hat{H} - E|D_{\mathbf{i}}\rangle\,C_{\mathbf{i}}(\tau) - \sum_{\mathbf{j}} \delta\tau\,\langle D_{\mathbf{i}}|\hat{H}|D_{\mathbf{j}}\rangle\,C_{\mathbf{j}}(\tau) = C_{\mathbf{i}}(\tau + \delta\tau). \quad (16)$$

This equation can be solved stochastically by sampling the population dynamics of a set of walkers (psips) in the Hilbert space of the system, which undergo the following processes [21]:

(1) spawning from $|D_{\mathbf{i}}\rangle$ to $|D_{\mathbf{j}}\rangle$ with probability:

$$p_{\mathrm{spawn}}(\mathbf{j}|\mathbf{i}) \propto \delta\tau|H_{\mathbf{ij}}|; \quad (17)$$

(2) death with probability:

$$p_{\mathrm{death}}(\mathbf{i}) \propto \delta\tau|H_{\mathbf{ii}} - S|; \quad (18)$$

(3) annihilation of particles of opposite sign on the same determinant.

In the death step, the shift S replaces the unknown exact energy E. This acts as a population control parameter and, once the system has reached a steady state, converges to the true energy. Another estimator for E is the projected energy:

$$E_{\mathrm{proj}} = \frac{\langle D_0|\hat{H}|\Psi\rangle}{\langle D_0|\Psi\rangle} = \sum_{\mathbf{i}\neq 0} \frac{N_{\mathbf{i}}^{\mathrm{CI}} H_{\mathbf{i}0}}{N_0}. \quad (19)$$

A set of equations like Eq. (14) holds for the CC wave function given in Eq. (1). Since $\langle D_{\mathbf{i}}|\Psi_{\mathrm{CC}}\rangle = t_{\mathbf{i}} + \mathcal{O}(t^2)$, we can write

$$t_{\mathbf{i}}(\tau) - \delta\tau\,\langle D_{\mathbf{i}}|\hat{H} - E|\Psi_{\mathrm{CC}}\rangle \approx t_{\mathbf{i}}(\tau + \delta\tau). \quad (20)$$

This can be described stochastically by the same three processes considered for FCIQMC, leading to an algorithm known as CCMC [22]. However, one must also consider contributions from composite clusters. For example,

$$\left\langle D_{ij}^{\alpha\beta}\right|\left.\Psi_{\mathrm{CC}}\right\rangle = t_{ij}^{\alpha\beta} + t_i^\alpha t_j^\beta - t_i^\beta t_j^\alpha\,, \quad (21)$$

and therefore, any of these three terms may contribute to death on $t_{ij}^{\alpha\beta}$ or to spawning onto some excitor coupled to it by the Hamiltonian. The selection process is therefore somewhat more complicated than for FCIQMC, originally consisting of the steps below [22]:

(1) a cluster size s is selected with probability:

$$p(s) = \frac{1}{2^{s+1}}; \quad (22)$$

(2) a particular cluster of s distinct excitors is selected with probability:

$$p(e|s) = s! \prod_{i=1}^{s} \frac{|N_i|}{|N_{\mathrm{ex}}|}; \quad (23)$$

where N_{ex} is the total population on excitors. The total selection probability is therefore

$$p_{\mathrm{sel}}(e) = p(e|s)p(s). \quad (24)$$

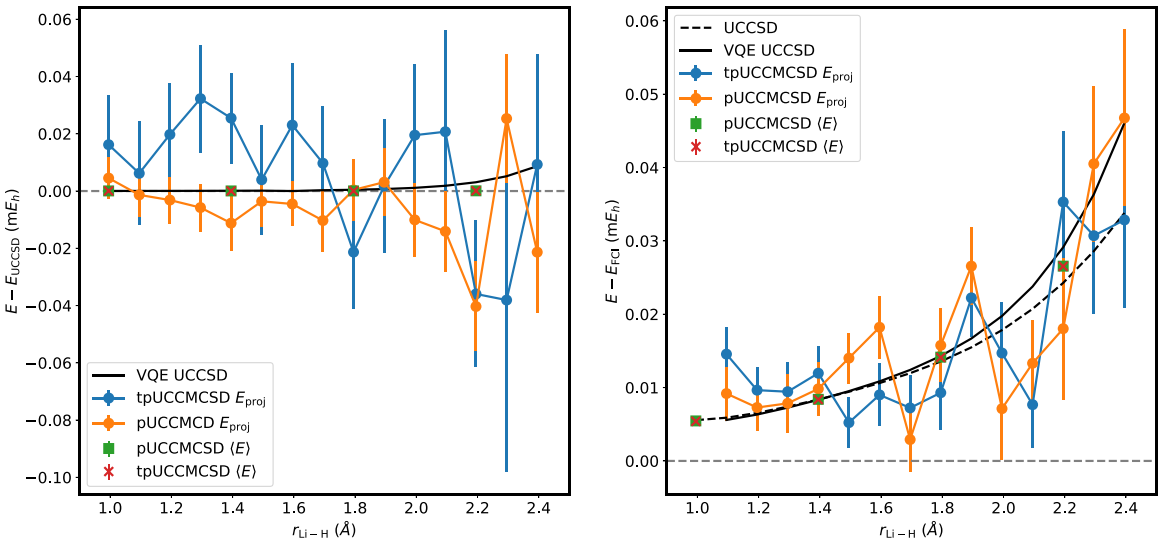

FIG. 2. Frozen core (left) and all-electron (right) LiH STO-3G energies, computed with pUCCMCSD (orange circles = projected energy, green squares = variational energy) and tpUCCMCSD (blue circles = projected energy, red crosses = variational energy). In the left panel, the black line corresponds to UCCSD VQE. In the right figure, the black dashed line corresponds to the deterministic UCCSD benchmark of Cooper and Knowles [45] and the black solid line line to UCCSD VQE. In both cases, the stochastic energies agree with the VQE results to within 50 μE_h.

Improvements have since been made to this selection algorithm to better importance-sample the wave function [38].

Recently, some of us have implemented a stochastic version of UCC and its Trotterized approximation [20], the details of which are expanded upon in the following section.

1. Projected UCCMC

While the UCC wave function is generally found by variationally optimizing the parameters, it is also possible [39,40] to solve a set of projected UCC (pUCC) equations:

$$\langle D_{\mathbf{i}}|\hat{H} - E|\Psi_{\text{UCC}}\rangle = 0. \tag{25}$$

This projective method is naturally more amenable to the QMC algorithms described above, as it leads to similar population dynamics to those in Eq. (20). However, the presence of de-excitation operators $\hat{T}^\dagger$ in the full UCC *Ansatz* substantially changes the structure of the allowed clusters, removing the constraint that cluster sizes must be at most equal to the maximum excitation level considered in the calculation. However, the expansion can be truncated to a finite cluster size which, if large enough, does not significantly affect the accuracy of the obtained answer. The selection scheme for UCCMC is then as follows:

(1) Select a cluster size s with probability $p(s) = \frac{1}{2^{s+1}}$.

(2) For all but the first excitor in the cluster, decide with probability $\frac{1}{2}$ whether it will be an excitation or de-excitation operator.

(3) A particular cluster is selected as before, with probability given by Eq. (23).

Having selected the cluster, it undergoes stochastic spawning and death as before. Overall, this constitutes the projected UCCMC (pUCCMC) algorithm. The final aspect one must be careful of is the projection of the wave function onto the HF reference, as this includes contributions beyond the reference population. This projection may be sampled stochastically during the course of the calculation concurrently with the reference population and the $\frac{N_{\mathbf{i}}^{\text{CI}} H_{\mathbf{i}0}}{N_0}$ terms.

2. Trotterized pUCCMC

Consider once again the Trotterized UCC *Ansatz* with $\rho = 1$:

$$|\Psi_{\text{tUCC}}\rangle = \prod_{\mathbf{n}} \exp[t_{\mathbf{n}}(\hat{\tau}_{\mathbf{n}} - \hat{\tau}_{\mathbf{n}}^\dagger)]|\Psi_0\rangle. \tag{26}$$

This *Ansatz* now depends on the order of excitors in the product, with different orders leading to different cluster amplitudes and potentially different energy values [41]. In recent

TABLE I. Size of the totally symmetric Σ^+ UCCSD Hilbert space and number of amplitudes above different thresholds for LiH in the STO-3G basis at a range of bond lengths, together with the percentage of the correlation energy recovered using each of the thresholds as a cutoff for amplitudes included in the VQE UCCSD *Ansatz*, relative to the completer VQE UCCSD calculation.

Bond length (Å)	Σ^+ UCCSD Hilbert Space	$t > 0.1$	% E_{corr}	$t > 0.01$	% E_{corr}	$t > 0.001$	% E_{corr}
0.995	35	0	0	8	97.43	29	99.93
1.395	35	1	71.20	8	98.75	19	99.94
1.795	35	1	70.54	8	98.94	22	99.95
2.195	35	3	88.90	8	99.13	25	99.99

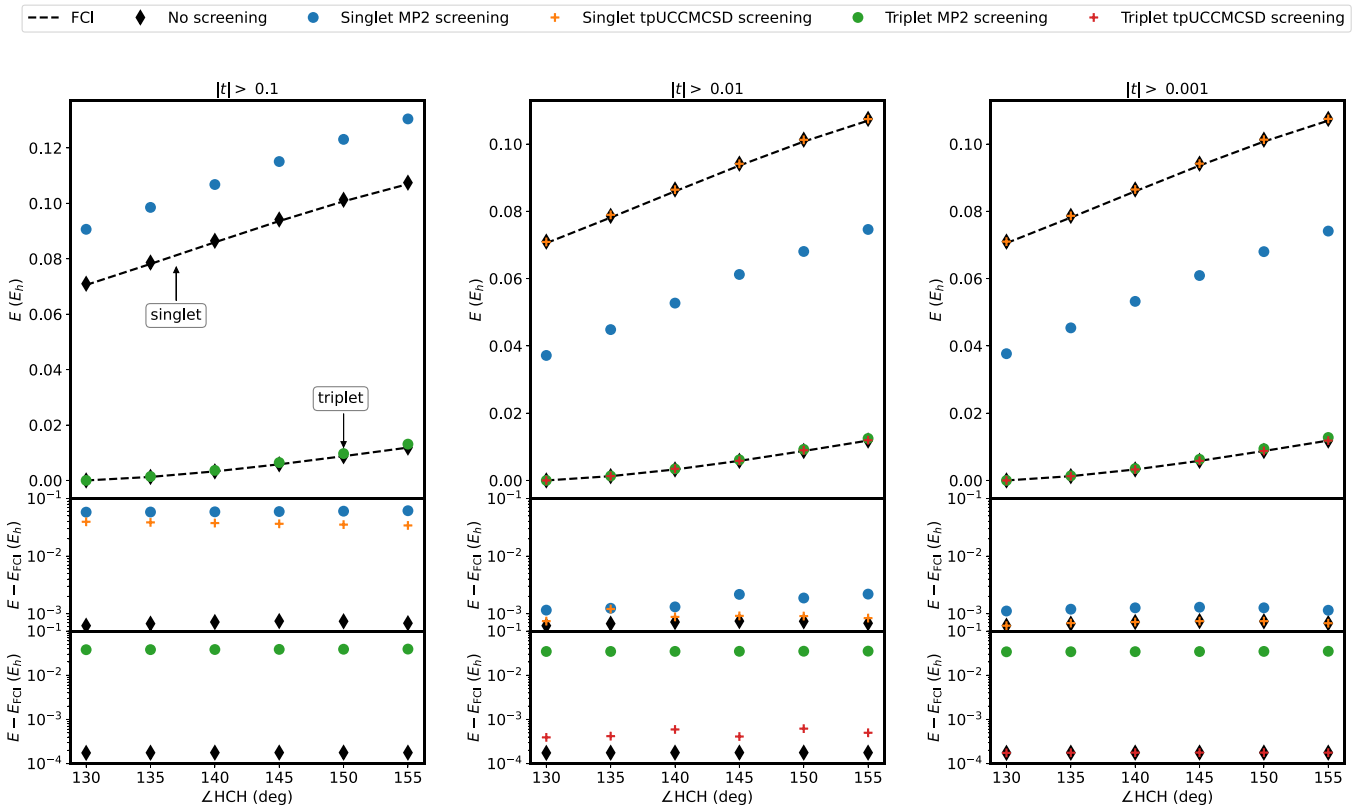

FIG. 3. CH_2 singlet and triplet energy computed with UCCSD VQE across the bending mode at $r_{CH} = 1.08$ Å with different coefficient thresholds, using MP2 (blue and green circles) and tpUCCMCSD (orange and red pluses) as screening methods. From left to right, we consider coefficients >0.1, 0.01, and 0.001, respectively. All energies in the top panel are relative to the lowest computed energy along the binding curve obtained with the same method—in this case, the triplet energy at $\angle HCH = 130^\circ$. For all methods, the error relative to FCI is given in the middle (for the singlet) and bottom (for the triplet) panels. In tpUCCMCSD screening, there are no amplitudes $|t| > 0.1$ for the triplet state.

work, Evangelista *et al.* [28] have defined an optimal ordering that guarantees complete wave function expressibility in this framework. Applying $\exp[t_i(\tau_i - \tau_i^\dagger)]$ to an arbitrary single determinant wave function $|\Psi\rangle$ leads to three possibilities:

(1) $\hat{\tau}_\mathbf{i}^\dagger |\Psi\rangle = 0$ and $\hat{\tau}_\mathbf{i} |\Psi\rangle \neq 0$:

$$\exp[t_\mathbf{i}(\hat{\tau}_\mathbf{i} - \hat{\tau}_\mathbf{i}^\dagger)] |\Psi\rangle = \cos(t_\mathbf{i}) |\Psi\rangle + \sin(t_\mathbf{i}) |\Psi_\mathbf{i}\rangle , \quad (27)$$

where $|\Psi_\mathbf{i}\rangle$ is the result of applying the excitation to $|\Psi\rangle$;

(2) $\hat{\tau}_\mathbf{i}^\dagger |\Psi\rangle \neq 0$ and $\hat{\tau}_\mathbf{i} |\Psi\rangle = 0$:

$$\exp[t_\mathbf{i}(\hat{\tau}_\mathbf{i} - \hat{\tau}_\mathbf{i}^\dagger)] |\Psi\rangle = \cos(t_\mathbf{i}) |\Psi\rangle - \sin(t_\mathbf{i}) |\Psi^\mathbf{i}\rangle , \quad (28)$$

TABLE II. Size of the totally symmetric UCCSD Hilbert space and number of amplitudes above different thresholds for triplet CH_2 in STO-3G at a range of CH bond lengths, with $\angle HCH = 135^\circ$.

Bond length (Å)	UCCSD Hilbert Space	$t > 0.1$	$t > 0.01$	$t > 0.001$
1.06	31	0	24	30
1.08	31	0	25	30
1.10	31	0	26	29
1.12	31	0	26	29
1.14	31	0	25	29
1.16	31	0	26	30
1.18	31	0	26	29

where $|\Psi^\mathbf{i}\rangle$ is the result of applying the de-excitation to $|\Psi\rangle$; and

(3) $\hat{\tau}_\mathbf{i}^\dagger |\Psi\rangle = 0$ and $\hat{\tau}_\mathbf{i} |\Psi\rangle = 0$:

$$\exp[t_\mathbf{i}(\hat{\tau}_\mathbf{i} - \hat{\tau}_\mathbf{i}^\dagger)] |\Psi\rangle = |\Psi\rangle . \quad (29)$$

To translate this into a stochastic algorithm, for each excitor present in the wave function, the algorithm assesses which of the cases listed above is appropriate. If the excitor cannot be applied, the next excitor is considered. If the excitor can be applied, this is done with probability:

$$p_\text{excit} = \frac{|\sin(t)|}{|\sin(t)| + |\cos(t)|}, \quad (30)$$

and the cluster amplitude is multiplied by $\pm\sin(t)$. With probability $1 - p_\text{excit}$, the operator is not applied, and the cluster amplitude is multiplied by $\cos(t)$. The cluster then undergoes the same spawning, death, and annihilation steps as in traditional CCMC, leading to a Trotterized pUCCMC approach (tpUCCMC). As in the case of full pUCCMC, this *Ansatz* modifies the projection of the wave function onto the reference, making it different from the reference population. Depending on the ordering of the excitors, a closed form for this projection may be found, but in general, it can easily be sampled during the stochastic propagation.

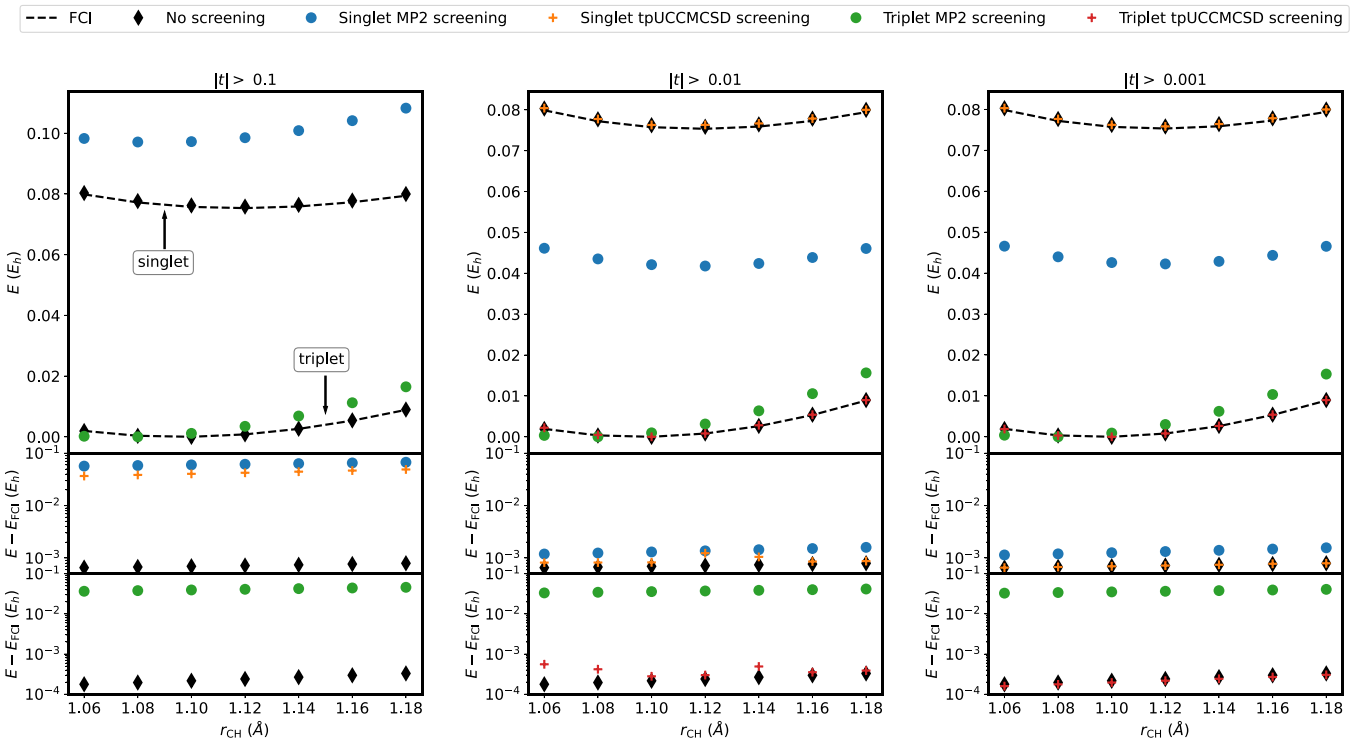

FIG. 4. CH_2 singlet and triplet energy computed with UCCSD VQE across the stretching mode at $\angle HCH = 135^\circ$ with different coefficient thresholds, using MP2 (blue and green circles) and tpUCCMCSD (orange and red pluses) as screening methods. From left to right, we consider coefficients >0.1, 0.01, and 0.001, respectively. All energies in the top panel are relative to the minimum energy along the binding curve obtained with the same method - in this case the triplet energy at $r_{CH} = 1.08$Å. For all methods, the error relative to FCI is given in the middle (for the singlet) and bottom (for the triplet) panels. In tpUCCMCSD screening, there are no amplitudes $|t| > 0.1$ for the triplet state.

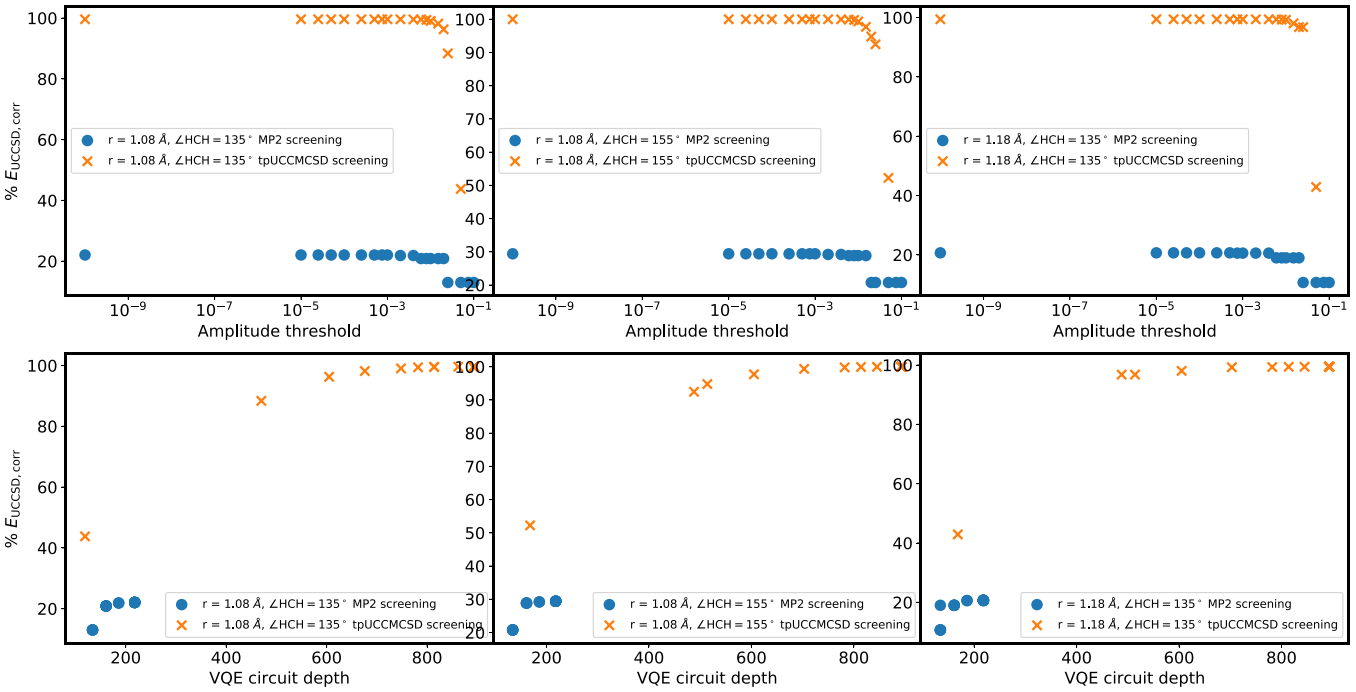

FIG. 5. Percentage of UCCSD correlation energy recovered for triplet CH_2 with MP2 (blue circles) and tpUCCMCSD (orange crosses) screening at a series of geometries. MP2 fails to converge for the triplet state, while tpUCCMCSD allows recovery of significant fractions of the correlation energy while reducing the circuit depth by up to half for all geometries.

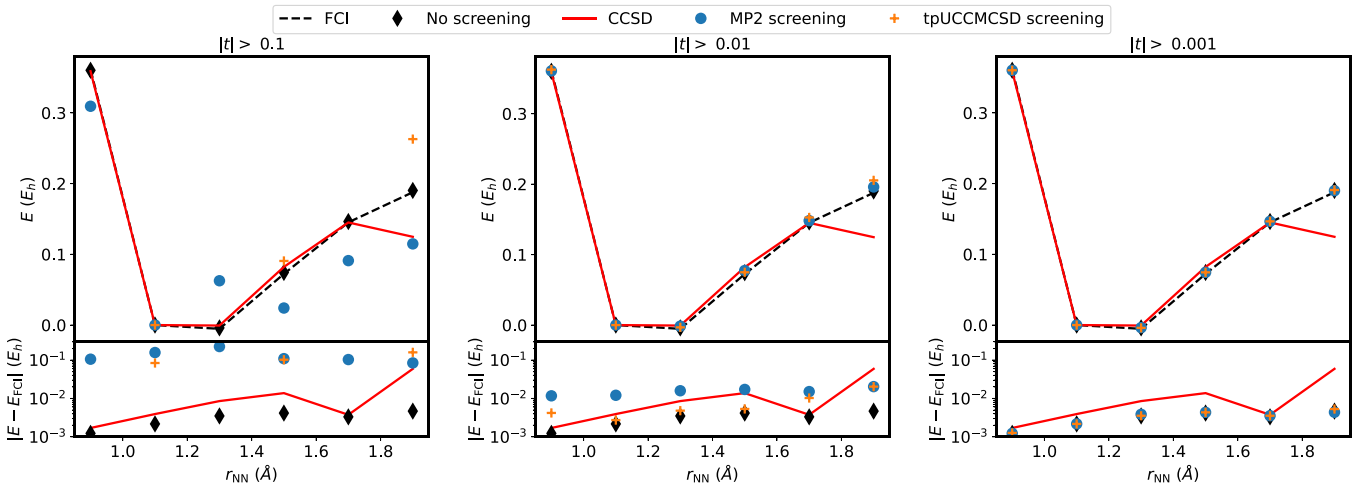

FIG. 6. N_2 frozen-core binding curve computed with UCCSD VQE with different coefficient thresholds, using MP2 (blue cicles) and tpUCCMCSD (orange crosses) screening. From left to right, we consider coefficients >0.1, 0.01, and 0.001, respectively. All energies in the top panel are relative to the energy at $r_{NN} = 1.1$ Å obtained with the same method. Energies converge to the unscreened UCCSD VQE value (solid black line) with number of parameters for both methods. At intermediate screening, tpUCCMCSD performs better than MP2 at compressed bond lengths. CCSD energies (red line) are shown for comparison.

D. Technical details

The VQE calculations have been performed using a minimal (STO-3G) basis set for all molecular species considered. Molecular integrals and molecular orbital coefficients have been obtained using the PySCF package [42]. The wave function *Ansatz* has been encoded into quantum circuits on a qubit register using the Jordan-Wigner scheme in the EUMEN program. For the optimization loop in the VQE procedure, the L-BFGS method has been applied. The state vector simulator Qulacs [43] has been used to evaluate the quantum circuits.

All QMC calculations have been carried out in a development version of HANDE-QMC [44]. Where directly compared, VQE and tpUCCMC calculations use the same ordering of excitors, applying all single (de)excitation operators ahead of the doubles. For triplet states, restricted open-shell HF reference states were used for all MC, MP2, and VQE calculations. All screened VQE UCCSD calculations used the relevant tpUCCMCSD/MP2 amplitudes as starting values for the parameters.

III. RESULTS

In this section, we assess the viability of the tpUCCSD method as a screening technique for UCCSD-based VQE. Given one method is based on a projective approach, while the other is variational, we first ascertain whether the wave functions obtained by the two approaches are sufficiently similar for tpUCCSD amplitudes to be a good predictor of VQE UCCSD amplitudes. To assess this, we turn our attention to the LiH molecule. In the STO-3G basis, this system consists of four electrons in 12 spin-orbitals, which can easily be treated by both VQE and tpUCCMCSD. The system can be further simplified by freezing the core Li 1*s* electrons. As seen in Fig. 2, in both cases, the energies obtained by the two methods agree within 50 μE_h for both the expectation value and the projected energy for tpUCCMCSD.

However, for tpUCCMCSD predictions to be useful as a starting guess or screening for VQE UCCSD amplitudes, the methods must agree not only in energy but also in individual cluster amplitudes. For this agreement to be achieved, care must be taken that the same ordering is used in both *Ansätze*. While for such small systems any arrangement of the excitors in the Trotterized UCC wave function will be able to describe the ground state wave function, the individual amplitudes may vary extensively, particularly in the more highly correlated regime, see the Supplemental Material [46]. For frozen core LiH, the tpUCCMCSD amplitudes agree with their deterministic counterparts within the 1σ-error bars.

Having convinced ourselves that the VQE UCCSD and tpUCCMCSD results are compatible, we investigate the potential of the latter as a screening technique for the former. Table I gives the number of amplitudes in the LiH wave function of different orders of magnitude in a stochastic snapshot of the tpUCCMCSD expansion. We find that the lowest threshold ($t > 0.001$) recovers >99.9% of the correlation energy at all geometries, while decreasing the size of the considered Hilbert space by 14–43%.

Even $t > 0.01$ generally recovers >97% of the correlation energy in all cases, despite only using eight parameters.

Following on from these results, we investigate the applicability of tpUCCMC-screened VQE to a series of small molecules in different scenarios: CH_2, which has a triplet ground state; N_2, which becomes increasingly strongly correlated as the bond between the nitrogen atoms is broken; and N_2H_2, where there is a crossing of diabatic states as it rotates from a *trans* to a *cis* geometry. In all cases, we use a snapshot of the amplitudes at the end of a short tpUCCMCSD run for screening.

For CH_2, considered with frozen 1*s* electrons on the C atom, we once again observe good agreement between tpUCCMCSD and VQE energies and wave functions, provided the same excitor ordering is used throughout, see the Supplemental Material [46]. In this paper, we consider

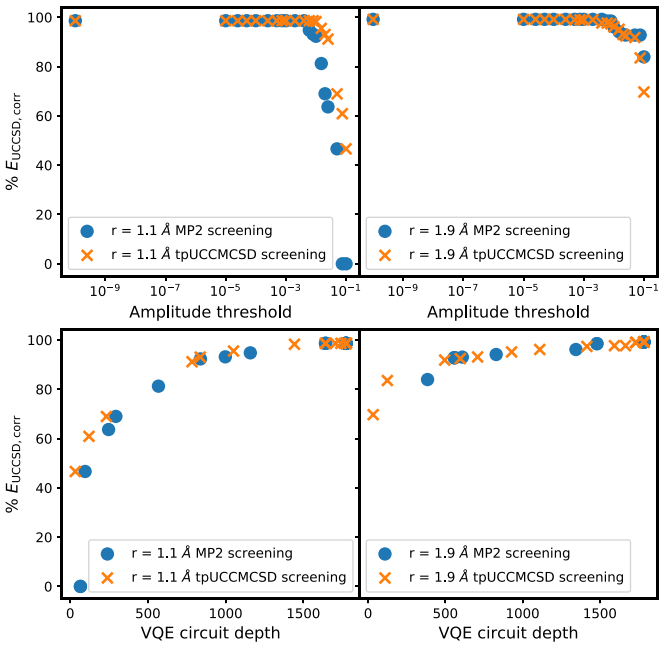

FIG. 7. Percentage of UCCSD correlation energy recovered for N_2 with MP2 (blue circles) and tpUCCMCSD (orange crosses) screening near equilibrium (left) and for a stretched bond (right). Performance is comparable between the two methods, with tpUCCMC exhibiting slightly faster convergence in terms of both threshold and depth.

both the symmetric stretch at an angle $\angle HCH = 135^\circ$ and the bend with $r_{CH} = 1.08$ Å, close to the experimental equilibrium geometry ($\angle HCH = 133.9^\circ$, $r_{CH} = 1.075$ Å) [47]. In this case, the tpUCCMCSD amplitudes are less spread out in magnitude, and therefore, the screening is less efficient at decreasing the number of VQE parameters to be considered (see Table II for an example). As expected from this distribution of amplitudes, screening at either $t > 0.01$ or $t > 0.001$ gives errors of <1 mE_h relative to the full UCCSD VQE calculation, for both singlet and triplet CH_2. Using MP2 as a screening method is competitive for the singlet state (see Figs. 3 and 4), while for the triplet, the MP2-screened results exhibit a systematic error of >10 mE_h which persists across all screening thresholds. Even when considering relative energies, MP2-screened calculations overestimate the energy of the triplet as the C-H bonds are stretched, as seen in Fig. 4, and generally underestimate the singlet-triplet gap. Considering quantum resources, we note that the tpUCCMC screening described above leads to significant depth reduction with relatively little correlation loss, as can be seen in Fig. 5, which also highlights the unsuitable quality of MP2-screened results independently of circuit depth.

The N_2 molecule as it approaches dissociation is one of the archetypal examples of static correlation and poses significant challenges to methods such as CC, which are based around the assumption that a single determinant dominates the wave function. For example, for $r_{NN} > 3.6a_0$, CCSD(T) [48] overestimates the correlation energy and diverges as the bond length is increased [49]. As can be seen in Fig. 6, the unitary, variationally optimized *Ansatz* avoids the failure of the traditional CCSD *Ansatz*, with the energy consistently above the FCI value and generally lower errors. In this case, both MP2 and tpUCCMCSD screening provide similar quality results, but the system highlights a few interesting differences between the two methods. First, in the left panel of Fig. 6, we observe that, while in MP2 there are consistently some amplitudes allowed by the screening, tpUCCMCSD does not have any amplitudes >0.1 for half of the geometries considered. As such, the screened method cannot provide any improvement over HF. Obviously, this threshold is too high, and the results obtained with either MP2 or tpUCCMCSD screening all have significant systematic and nonparallelity errors (10–500 mE_h), making it inappropriate for the treatment of this system.

Secondly, in the previous examples, we have generally found that tpUCCMCSD screening converges slightly faster with screening threshold than MP2, or indeed MP2 fails to converge at all. In this case, we find that tpUCCMCSD converges faster than MP2 for compressed bonds, but they are comparable in the stretched regime, as is further highlighted in Fig. 7, which shows that, once again, screening can be used to meaningfully reduce circuit depth without significant accuracy loss. The behavior can be correlated to the number of amplitudes in the *Ansatz* at each geometry, with tpUCCMCSD including more parameters at shorter bond lengths than MP2 (see Table III). Both of these features emphasize the fact that a constant amplitude threshold does not necessarily generate a consistent number of parameters across all geometries of a given system. Where consistency is desirable, which will often be the case when constructing a description of a physical system, a threshold based directly on the number of parameters included may be preferable, although it is not without its own challenges, as we discuss below.

Finally, the energy landscape of the *cis-trans* interconversion of N_2H_2 allows us to investigate another highly

TABLE III. Size of the totally symmetric UCCSD Hilbert space and number of amplitudes above different thresholds for frozen core N_2 in STO-3G at a range of bond lengths, screened with both MP2 and tpUCCMCSD.

Bond length	UCCSD Hilbert	tpUCCMCSD			MP2		
(Å)	space	$t > 0.1$	$t > 0.01$	$t > 0.001$	$t > 0.1$	$t > 0.01$	$t > 0.001$
0.9	54	0	36	52	2	24	53
1.1	54	2	44	52	2	26	49
1.3	54	0	42	53	2	30	49
1.5	54	3	47	53	4	35	53
1.7	54	0	42	53	8	39	53
1.9	54	2	34	52	12	41	53

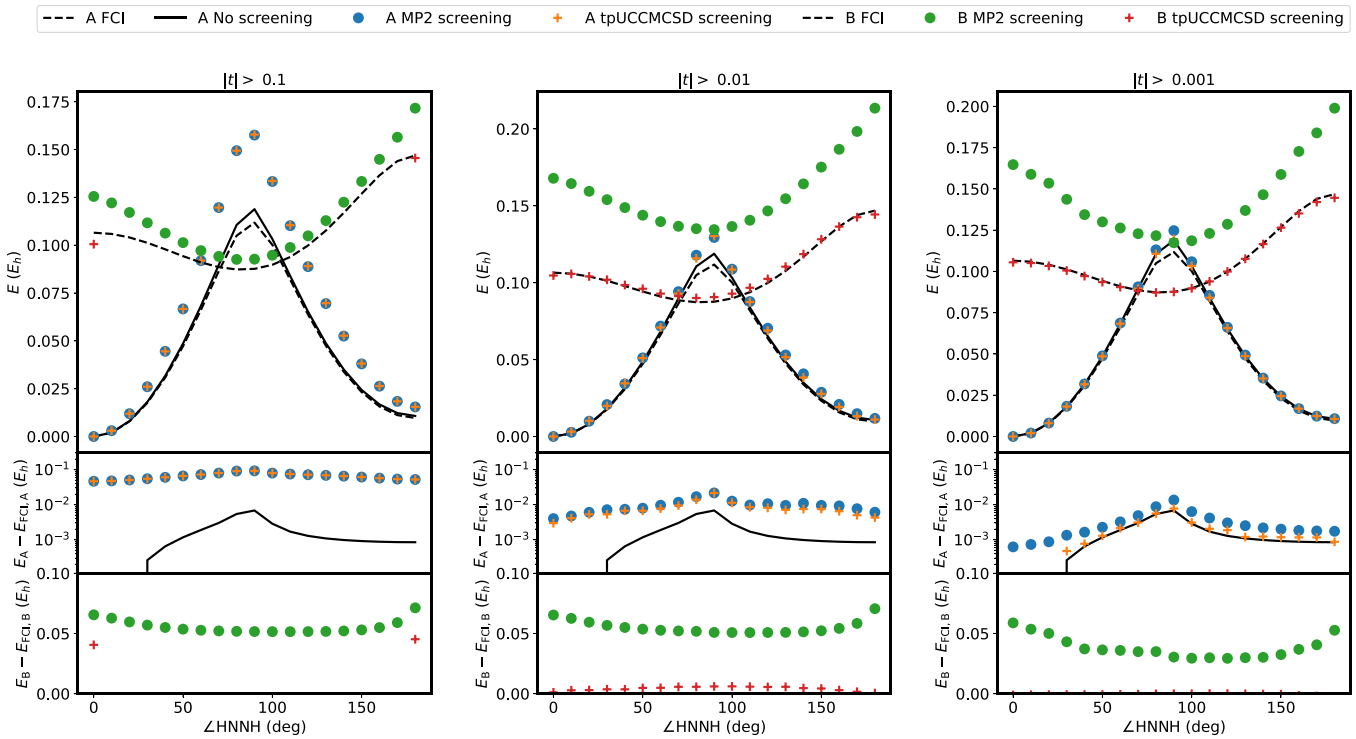

FIG. 8. N_2H_2 energy computed with UCCSD VQE with different coefficient thresholds, using MP2 (blue and green circles) and tpUCCMCSD (orange and red crosses) for screening. We consider two states, a closed-shell singlet state of A symmetry in the C2 point group and a triplet state of B symmetry. The A state is the ground state around the *cis* and *trans* geometries of N_2H_2, but the triplet becomes favored around a rotation angle of 90°. From left to right, we consider coefficients >0.1, 0.01, and 0.001, respectively. In all cases, the energies in the top panel are quoted relative to the energy of the singlet state in the *trans* geometry, computed with the same method. For the A state, as with all singlet molecules so far, both MP2 and tpUCCMCSD converge toward the true UCCSD energy, although in this case, at 0.001, MP2 is noticeably worse than tpUCCMCSD. For the B state, however, MP2 is unable to capture the correlation and does not improve with added amplitudes. This gives unphysical results, with the B state higher in energy than the A state for all geometries except ∠HNNH = 90° even at the lowest threshold considered.

TABLE IV. Size of the UCCSD Hilbert space and number of tpUCCMCSD amplitudes above different thresholds for the lowest singlet and triplet N_2H_2 states in STO-3G at a range of dihedral ∠HNNH.

State	Dihedral angle (deg)	UCCSD Hilbert Space	$t > 0.1$	$t > 0.01$	$t > 0.001$
A	0	100	1	46	90
	30	185	1	60	170
	60	185	1	71	166
	90	185	1	65	175
	120	185	1	65	161
	150	185	1	56	172
	180	100	1	42	97
B	0	83	1	40	77
	30	160	0	44	140
	60	160	0	51	147
	90	160	0	49	150
	120	160	0	51	149
	150	160	0	45	147
	180	83	1	36	76

correlated regime around the transition state of this transformation. For simplicity, we investigate the rotation about the nitrogen-nitrogen bond starting from the equilibrium geometry of *trans* N_2H_2 [50], without allowing any relaxation of other geometrical parameters. At the HF level, the singlet state of this system would be characterized by two diabatic states which cross at 86.8(1)°, see the Supplemental Material [46]. This introduces an unphysical discontinuity in the energy surface, which often remains even after the application of further correlated methods [51]. To be able to treat this system using VQE, we freeze the eight lowest-energy electrons. The resulting system exhibits an additional interesting feature as two FCI states of different spatial symmetry cross, as can be seen in Fig. 8. The conservation of various symmetries—spin, particle number, and point group—in quantum circuits is an interesting problem, and in this system, it turns out to be crucial for the correct description of the energy surface. Not enforcing point group symmetry leads to a very compelling yet unphysical state which transitions smoothly from the A to the B state as the system approaches a 90° rotation.

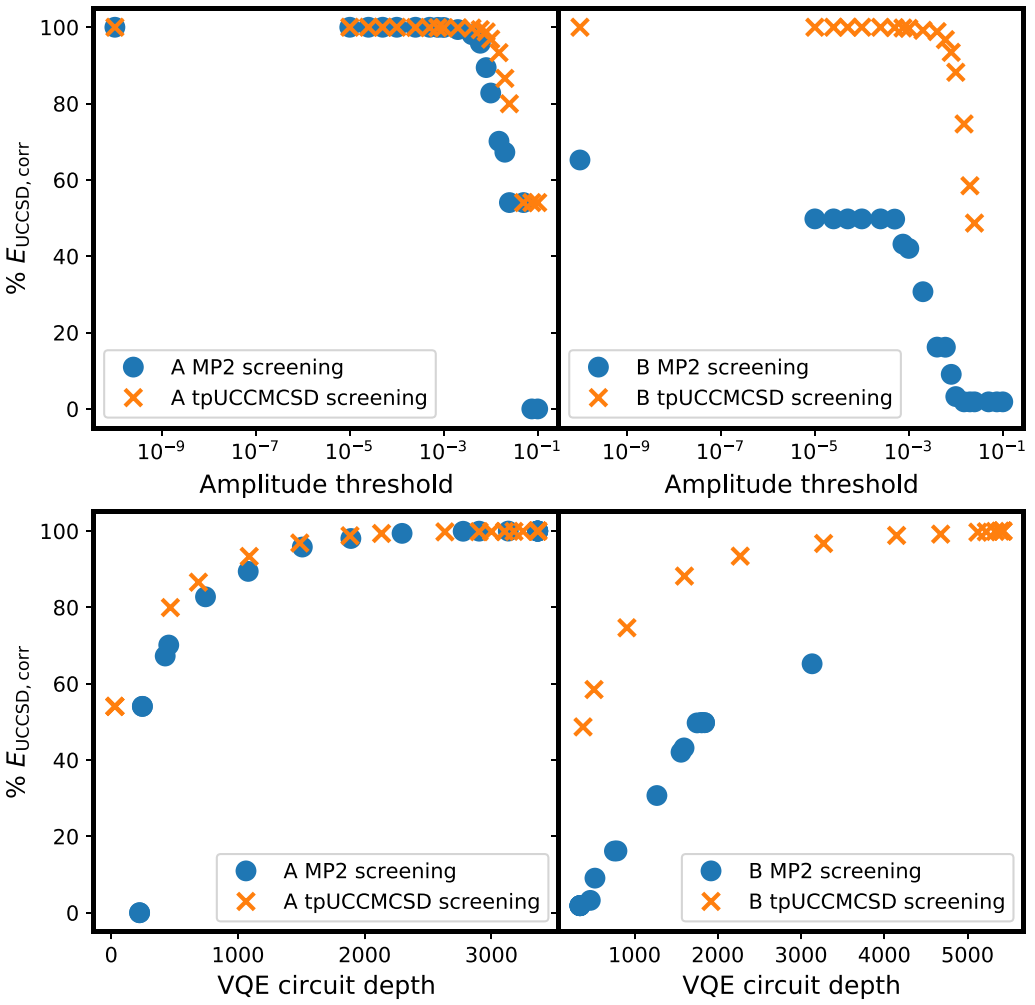

FIG. 9. N_2H_2 percentage of UCCSD correlation energy recovered with MP2 (blue circles) and tpUCCMCSD (orange crosses) screening for the A state at the *trans* geometry (left) and the B state at $\angle$HCH $= 90^\circ$ (right) as a function of screening threshold (top) and circuit depth (bottom). tpUCCMCSD outperforms MP2 over the entire range of screening thresholds, and for the triplet B state, any MP2-screened state fails to converge to the correct energy.

Once point group symmetry constraints are considered, VQE based on the UCCSD *Ansatz* with the excitation symmetry filtered correctly reproduces the behavior observed in the exact surface; however, starting from an $m_s = 0$ open-shell HF reference or an $m_s = 1$ reference leads to different energies for the B state. For the rest of our analysis, we focus on the $m_s = 0$ A state and the $m_s = 1$ B state, which correspond to the two lowest-energy states in the system. The orders of magnitude of amplitudes in a short tpUCCMCSD run for this system at various rotation angles are given in Table IV. This system exhibits many of the behaviors we noted in smaller examples. For the singlet state, both MP2- and tpUCCMCSD-screened UCCSD VQE converge to the correct UCCSD energy with increasing number of amplitudes, but for the triplet state, MP2 fails to converge, retaining an error of at least 30 mE_h even for the lowest threshold, see Fig. 8. As there is no systematic error in the singlet state, this causes MP2 screening to predict the wrong ordering of the singlet and triplet states for rotation angles $\sim 90^\circ$.

Figure 9 shows the convergence of VQE UCCSD energy as a function of amplitude threshold and circuit depth for the A state at 0° and the B state at 90°. This highlights the same trend as before, with tpUCCMCSD screening only slightly more efficient than MP2 as a function of screening threshold for the singlet state but clearly superior for the triplet. In both cases, using tpUCCMCSD, it is possible to recover $>90\%$ of the correlation energy with a circuit that is only half as deep as the full VQE UCCSD implementation. In Fig. 10, we consider the correlation energy for the *trans* geometry of N_2H_2 and the transition state at 90° directly as a function of the number of parameters in the UCCSD expansion, using the truncation order from tpUCCMCSD. Due to the change in point group symmetry from $C_{2h}(C_{2v})$ at the *trans*(*cis*) geometry to C_2 along the rest of the binding curve, the number of possible parameters is halved at the ends. Therefore, where the symmetry of the system changes, computations based on a constant number of amplitudes are nontrivial to implement.

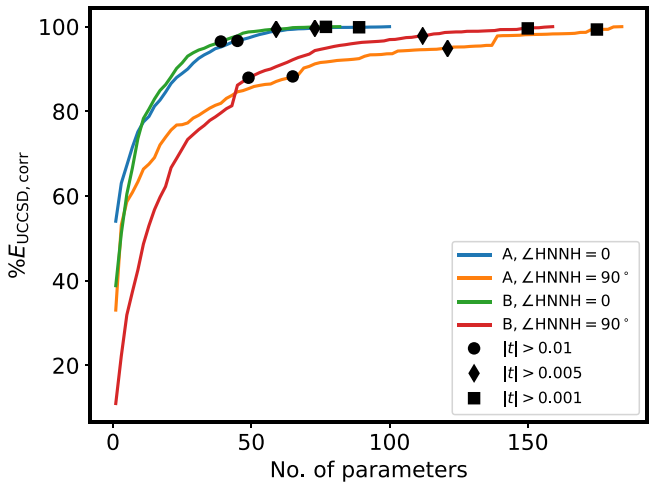

FIG. 10. Convergence of the correlation energy with number of UCCSD amplitudes in the lowest-lying electronic states of N_2H_2 at $\angle$HNNH $= 0^\circ$ and 90°. The percentage of the energy recovered monotonically increases with parameter number, but a large fraction is encoded within the first few parameters to be included. Behavior is similar between the two states at matching geometries, dominated by the difference in the maximum number of parameters rather than the different degrees of correlation character in the two states. Some corresponding amplitude thresholds are marked for comparison.

As a final point, we consider the scaling of such screening methods with basis set size. While the VQE method, even simulated on a classical machine, is currently limited to a minimal basis for the systems considered here, the sparse tpUCCMC approach can tackle more basis functions. Given results from this method have been shown to agree well with VQE, we use them to predict its expected behavior. We consider the N_2 molecule in the cc-pVDZ, cc-pVTZ, and cc-pVQZ basis sets. We start by running a tpUCCMCSD calculation for these systems to convergence. We then truncate the resulting parameter sets and rerun the calculation in this limited Hilbert space. Results are given in Table V. In all cases, the correlation energy increases with the number of amplitudes included, but we find that >85% of it is accounted for at a threshold of $|t| > 0.001$ in all cases. While at this value the number of amplitudes required increases with basis set size, the proportion of the Hilbert space decreases, suggesting larger relative resource reductions are possible for larger basis sets.

IV. CONCLUSIONS

We have shown that UCCMC can be used successfully as a screening method for UCCSD-based VQE, with short, potentially unconverged stochastic runs providing a set of amplitudes that may be truncated at a given coefficient threshold before being further optimized by VQE. We expect the method would also be compatible with the recently developed projected quantum eigensolver [52]. Importantly, the classical screening approach is entirely a preprocessing step, so requires no additional quantum resources.

Standard noise models such as amplitude and phase damping [53] predict exponential decay of the quantum signal with time, controlled by the relaxation time T_1 and dephasing time T_2 [54]. Significantly reducing the depth and therefore the computation time of the VQE circuit, as we have seen is possible for N_2H_2, where >90% of the correlation energy could be recovered with half the circuit depth, would therefore lead to a major reduction in the error rates observed on real hardware. Furthermore, two-qubit gates such as CNOTs are responsible for most gate noise on current devices. The number of such gates is reduced proportionally to the number of parameters removed in screened calculations. Errors in the single-qubit gates should also be reduced, as larger values for the angles in the R_z gates involved in the UCC *Ansatz* are easier to implement with high fidelity than lower values.

We have compared tpUCCMC screening with the preexistent MP2-based screening approach. In the case of singlet states, the results using UCCMC for screening are seen to converge slightly faster with screening threshold than the corresponding MP2-screened values. For triplets, we have found that the MP2-screened calculations fail to converge to the true ground state at all. This highlights the fact that tpUCCMC screening can be easily applied to any molecular system, while more care is needed when considering

TABLE V. Screened N_2 UCCMCSD correlation energy E_{corr} and number of parameters N_p as a function of basis set and screening threshold. In all cases, >85% of the correlation energy can be recovered using a threshold of $|t| > 0.001$, which corresponds to a decreasing proportion of the Hilbert space as the size of the basis increases. In the cc-pVQZ basis set, 98% of the correlation energy can be recovered with only 44% of parameters.

	$t > 0.1$		$t > 0.05$		$t > 0.01$		$t > 0.005$	
Basis set	E_{corr}	N_p	E_{corr}	N_p	E_{corr}	N_p	E_{corr}	N_p
cc-pVDZ	−0.0799(6)	3	−0.0980(5)	5	−0.260(1)	205	−0.3272(4)	607
cc-pVTZ	−0.073(3)	3	−0.089(2)	5	−0.2413(6)	226	−0.300(1)	611
cc-pVQZ	−0.034(1)	2	−0.091(1)	8	−0.217(2)	239	−0.279(2)	762
	$t > 0.001$		$t > 0.0005$		$t > 0.0001$		All t	
Basis set	E_{corr}	N_p	E_{corr}	N_p	E_{corr}	N_p	E_{corr}	N_p
cc-pVDZ	−0.3570(7)	1547	−0.3592(5)	2047	−0.359(1)	3245	−0.3608(3)	4256
cc-pVTZ	−0.4127(5)	4544	−0.422(2)	7489	−0.4367(3)	15 701	−0.437(1)	26 420
cc-pVQZ	−0.426(3)	5897	−0.461(4)	12 413	−0.483(2)	43 345	−0.493(6)	97 994

whether MP2 is suitable for a particular application. Furthermore, tUCC amplitudes are often highly dependent on operator ordering in the cluster expansion. While tpUCCMC can be adapted to match any operator ordering, MP2 can only generate one set of amplitudes, which may be better or worse predictors for the corresponding tUCC values depending on the chosen order. For all molecules we have considered, the accuracy of the results increases monotonically with the number of amplitudes included in the *Ansatz*, allowing one to balance result quality with resource limitations as necessary.

tpUCCMCSD results for N_2 in increasingly large basis sets confirm our expectation that the benefits of such screening methods get more significant as one considers larger systems. While the Hilbert spaces required for UCC calculations will scale with high-order polynomials of the system size, a smaller fraction of the amplitudes in this space will have large coefficients and therefore contribute significantly to the energy, at least in the largely single-reference, dynamically correlated areas of the landscape where CC methods perform well. Furthermore, it has been shown that linear scaling CC can be achieved by careful screening of amplitudes by distance [55–59]. We expect that the Trotterized UCC approach and its stochastic counterpart will, in principle, be able to take advantage of this, especially on systems of multiple molecules, and propagate these gains forward into screened VQE calculations.

ACKNOWLEDGMENTS

M.-A.F. is grateful to the Cambridge Trust and Corpus Christi College for a studentship and A.J.W.T. to the Royal Society for a University Research Fellowship under Grant No. UF160398. The VQE numerical simulations in this paper were performed on Microsoft Azure Virtual Machines provided by the program Microsoft for Startups.

[1] D. S. Abrams and S. Lloyd, Simulation of Many-Body Fermi Systems on a Universal Quantum Computer, Phys. Rev. Lett. **79**, 2586 (1997).

[2] D. S. Abrams and S. Lloyd, Quantum Algorithm Providing Exponential Speed Increase for Finding Eigenvalues and Eigenvectors, Phys. Rev. Lett. **83**, 5162 (1999).

[3] A. Aspuru-Guzik, A. D. Dutoi, P. J. Love, and M. Head-Gordon, Chemistry: Simulated quantum computation of molecular energies, Science **309**, 1704 (2005).

[4] A. Peruzzo, J. McClean, P. Shadbolt, M. H. Yung, X. Q. Zhou, P. J. Love, A. Aspuru-Guzik, and J. L. O'Brien, A variational eigenvalue solver on a photonic quantum processor, Nat. Commun. **5**, 4213 (2014).

[5] A. Kandala, A. Mezzacapo, K. Temme, M. Takita, M. Brink, J. M. Chow, and J. M. Gambetta, Hardware-efficient variational quantum eigensolver for small molecules and quantum magnets, Nature (London) **549**, 242 (2017).

[6] R. Wiersema, C. Zhou, Y. de Sereville, J. F. Carrasquilla, Y. B. Kim, and H. Yuen, Exploring entanglement and optimization within the Hamiltonian variational ansatz, PRX Quantum **1**, 020319 (2020).

[7] B. T. Gard, L. Zhu, G. S. Barron, N. J. Mayhall, S. E. Economou, and E. Barnes, Efficient symmetry-preserving state preparation circuits for the variational quantum eigensolver algorithm, npj Quantum Inf. **6**, 10 (2020).

[8] W. Kutzelnigg, Quantum chemistry in Fock space. I. The universal wave and energy operators, J. Chem. Phys. **77**, 3081 (1982).

[9] W. Kutzelnigg and S. Koch, Quantum chemistry in Fock space. II. Effective Hamiltonians in Fock space, J. Chem. Phys. **79**, 4315 (1983).

[10] W. Kutzelnigg, Quantum chemistry in Fock space. III. Particle-hole formalism, J. Chem. Phys. **80**, 822 (1984).

[11] R. J. Bartlett, S. A. Kucharski, and J. Noga, Alternative coupled-cluster *Ansätze* II. The unitary coupled-cluster method, Chem. Phys. Lett. **155**, 133 (1989).

[12] P. K. Barkoutsos, J. F. Gonthier, I. Sokolov, N. Moll, G. Salis, A. Fuhrer, M. Ganzhorn, D. J. Egger, M. Troyer, A. Mezzacapo *et al.*, Quantum algorithms for electronic structure calculations: Particle-hole Hamiltonian and optimized wave-function expansions, Phys. Rev. A **98**, 022322 (2018).

[13] C. Møller and M. S. Plesset, Note on an approximation treatment for many-electron systems, Phys. Rev. **46**, 618 (1934).

[14] J. Romero, R. Babbush, J. R. McClean, C. Hempel, P. J. Love, and A. Aspuru-Guzik, Strategies for quantum computing molecular energies using the unitary coupled cluster ansatz, Quantum Sci. Technol. **4**, 014008 (2018).

[15] M. Metcalf, N. P. Bauman, K. Kowalski, and W. A. De Jong, Resource-efficient chemistry on quantum computers with the variational quantum eigensolver and the double unitary coupled-cluster approach, J. Chem. Theory Comput. **16**, 6165 (2020).

[16] H. R. Grimsley, S. E. Economou, E. Barnes, and N. J. Mayhall, An adaptive variational algorithm for exact molecular simulations on a quantum computer, Nat. Commun. **10**, 3007 (2019).

[17] I. G. Ryabinkin, T.-C. Yen, S. N. Genin, and A. F. Izmaylov, Qubit coupled cluster method: A systematic approach to quantum chemistry on a quantum computer, J. Chem. Theory Comput. **14**, 6317 (2018).

[18] I. G. Ryabinkin, R. A. Lang, S. N. Genin, and A. F. Izmaylov, Iterative qubit coupled cluster approach with efficient screening of generators, J. Chem. Theory Comput. **16**, 1055 (2020).

[19] Y. Fan, C. Cao, X. Xu, Z. Li, D. Lv, and M.-H. Yung, Circuit-depth reduction of unitary-coupled-cluster ansatz by energy sorting, arXiv:2106.15210 (2021).

[20] M.-A. Filip and A. J. W. Thom, A stochastic approach to unitary coupled cluster, J. Chem. Phys. **153**, 214106 (2020).

[21] G. H. Booth, A. J. W. Thom, and A. Alavi, Fermion monte carlo without fixed nodes: A game of life, death, and annihilation in Slater determinant space, J. Chem. Phys. **131**, 054106 (2009).

[22] A. J. W. Thom, Stochastic Coupled Cluster Theory, Phys. Rev. Lett. **105**, 263004 (2010).

[23] J. E. Deustua, J. Shen, and P. Piecuch, Converging High-Level Coupled-Cluster Energetics by Monte Carlo Sampling and Moment Expansions, Phys. Rev. Lett. **119**, 223003 (2017).

[24] J. Čížek, On the correlation problem in atomic and molecular systems. Calculation of wavefunction components in Ursell-

type expansion using quantum-field theoretical methods, J. Chem. Phys. **45**, 4256 (1966).
[25] J. Čížek, On the use of the cluster expansion and the technique of diagrams in calculations of correlation effects in atoms and molecules, Adv. Chem. Phys. **24**, 35 (1969).
[26] H. F. Trotter, On the product of semi-groups of operators, Proc. Amer. Math. Soc. **10**, 545 (1959).
[27] M. Suzuki, Generalized Trotter's formula and systematic approximants of exponential operators and inner derivations with applications to many-body problems, Commun. Math. Phys. **51**, 183 (1976).
[28] F. A. Evangelista, G. K. L. Chan, and G. E. Scuseria, Exact parameterization of fermionic wave functions via unitary coupled cluster theory, J. Chem. Phys. **151**, 244112 (2019).
[29] P. Jordan and E. Wigner, Über das Paulische Äquivalenzverbot, Z. Phys. **47**, 631 (1928).
[30] S. B. Bravyi and A. Y. Kitaev, Fermionic quantum computation, Ann. Phys. **298**, 210 (2002).
[31] A. Cowtan, W. Simmons, and R. Duncan, A generic compilation strategy for the unitary coupled cluster ansatz, arXiv:2007.10515 (2020).
[32] S. McArdle, T. Jones, S. Endo, Y. Li, S. C. Benjamin, and X. Yuan, Variational ansatz-based quantum simulation of imaginary time evolution, npj Quantum Inf. **5**, 75 (2019).
[33] M. Motta, C. Sun, A. T. K. Tan, M. J. O'Rourke, E. Ye, A. J. Minnich, F. G. S. L. Brandão, and G. K.-L. Chan, Determining eigenstates and thermal states on a quantum computer using quantum imaginary time evolution, Nat. Phys. **16**, 205 (2020).
[34] D. A. Mazziotti, S. E. Smart, and A. R. Mazziotti, Quantum simulation of molecules without fermionic encoding of the wave function, New J. Phys. **23**, 113037 (2021).
[35] M. Cerezo, A. Sone, T. Volkoff, L. Cincio, and P. J. Coles, Cost function dependent barren plateaus in shallow parametrized quantum circuits, Nat. Commun. **12**, 1791 (2021).
[36] J. B. Anderson, A random-walk simulation of the Schrödinger equation: H3+, J. Chem. Phys. **63**, 1499 (1975).
[37] D. Ceperley and B. Alder, Quantum Monte Carlo, Science **231**, 555 (1986).
[38] C. J. C. Scott and A. J. W. Thom, Stochastic coupled cluster theory: Efficient sampling of the coupled cluster expansion, J. Chem. Phys. **147**, 124105 (2017).
[39] S. Pal, Use of a unitary wavefunction in the calculation of static electronic properties, Theor. Chim. Acta **66**, 207 (1984).
[40] F. A. Evangelista, Alternative single-reference coupled cluster approaches for multireference problems: The simpler, the better, J. Chem. Phys. **134**, 224102 (2011).
[41] H. R. Grimsley, D. Claudino, S. E. Economou, E. Barnes, and N. J. Mayhall, Is the Trotterized UCCSD ansatz chemically well-defined? J. Chem. Theory Comput. **16**, 1 (2020).
[42] Q. Sun, T. C. Berkelbach, N. S. Blunt, G. H. Booth, S. Guo, Z. Li, J. Liu, J. D. McClain, E. R. Sayfutyarova, S. Sharma *et al.*, PySCF: The Python-based simulations of chemistry framework, WIREs Comput. Mol. Sci. **8**, e1340 (2017).
[43] Y. Suzuki, Y. Kawase, Y. Masumura, Y. Hiraga, M. Nakadai, J. Chen, K. M. Nakanishi, K. Mitarai, R. Imai, S. Tamiya *et al.*, Qulacs: A fast and versatile quantum circuit simulator for research purpose, Quantum **5**, 559 (2021).
[44] J. S. Spencer, N. S. Blunt, S. Choi, J. Etrych, M.-A. Filip, W. M. C. Foulkes, R. S. T. Franklin, W. J. Handley, F. D. Malone, V. A. Neufeld *et al.*, The HANDE-QMC project: open-source stochastic quantum chemistry from the ground state up, J. Chem. Theory Comput. **15**, 1728 (2019).
[45] B. Cooper and P. J. Knowles, Benchmark studies of variational, unitary and extended coupled cluster methods, J. Chem. Phys. **133**, 234102 (2010).
[46] See Supplemental Material at http://link.aps.org/supplemental/10.1103/PhysRevResearch.4.023243 for examples of tpUCCMCSD amplitudes and N_2H_2 diabatic states.
[47] P. Jensen, P. R. Bunker, and A. R. Hoy, The equilibrium geometry, potential function, and rotation-vibration energies of CH_2 in the $\tilde{X}^3B_1$ ground state, J. Chem. Phys. **77**, 5370 (1982).
[48] K. Raghavachari, G. W. Trucks, J. A. Pople, and M. Head-Gordon, A fifth-order perturbation comparison of electron correlation theories, Chem. Phys. Lett. **157**, 479 (1989).
[49] G. K.-L. Chan, M. Kállay, and J. Gauss, State-of-the-art density matrix renormalization group and coupled cluster theory studies of the nitrogen binding curve, J. Chem. Phys. **121**, 6110 (2004).
[50] J. Demaison, F. Hegelund, and H. Bürger, Experimental and *ab initio* equilibrium structure of trans-diazene HNNH1, J. Mol. Struct. **413-414**, 447 (1997).
[51] P. Mach, J. Masik, J. Urban, and I. Hubač, Single-root multireference Brillouin-Wigner coupled-cluster theory. rotational barrier of the N_2H_2 molecule, Mol. Phys. **94**, 173 (1998).
[52] N. H. Stair and F. A. Evangelista, Simulating many-body systems with a projective quantum eigensolver, PRX Quantum **2**, 030301 (2021).
[53] M. A. Nielsen and I. L. Chuang, *Quantum Computation and Quantum Information: 10th Anniversary Edition* (Cambridge University Press, Cambridge, 2010).
[54] J. Ghosh, A. G. Fowler, and M. R. Geller, Surface code with decoherence: An analysis of three superconducting architectures, Phys. Rev. A **86**, 062318 (2012).
[55] G. E. Scuseria and P. Y. Ayala, Linear scaling coupled cluster and perturbation theories in the atomic orbital basis, J. Chem. Phys. **111**, 8330 (1999).
[56] M. Schütz and H.-J. Werner, Low-order scaling local electron correlation methods. IV. Linear scaling local coupled-cluster (LCCSD), J. Chem. Phys. **114**, 661 (2001).
[57] N. Flocke and R. J. Bartlett, A natural linear scaling coupled-cluster method, J. Chem. Phys. **121**, 10935 (2004).
[58] J. E. Subotnik, A. Sodt, and M. Head-Gordon, A near linear-scaling smooth local coupled cluster algorithm for electronic structure, J. Chem. Phys. **125**, 074116 (2006).
[59] C. Riplinger and F. Neese, An efficient and near linear scaling pair natural orbital based local coupled cluster method, J. Chem. Phys. **138**, 034106 (2013).